Crystal facet orientation and temperature dependence of charge and spin Hall effects in noncollinear antiferromagnets: A first-principles investigation

Meng Zhu, Xinlu Li,* Fanxing Zheng, Jianting Dong, Ye Zhou, Kun Wu, and Jia Zhang†
School of Physics and Wuhan National High Magnetic Field Center, Huazhong University of Science and Technology, 430074 Wuhan, China

(Received 26 May 2024; revised 26 July 2024; accepted 28 July 2024; published 9 August 2024)

Noncollinear antiferromagnets (nc-AFMs) have attracted increasing research attention in spintronics due to their unique spin structures and fascinating charge and spin transport properties. By using first-principles calculations, we comprehensively investigate the charge and spin Hall effects in representative noncollinear antiferromagnet Mn_3Pt. Our study reveals that the Hall effects in nc-AFMs are critically dependent on the crystal facet orientation and temperature. For (001)-oriented Mn_3Pt, each charge and spin Hall conductivity element comprises time-reversal odd (T-odd) and even (T-even) contribution, associated with longitudinal conductivity, which leads to sizable and highly anisotropic Hall conductivity. The temperature dependence of charge and spin Hall conductivity has been elucidated by considering both phonon and spin disorder scattering. The scaling relations between Hall conductivity and longitudinal conductivity have also been investigated. The existence of prominent spin Hall effect in nc-AFMs may generate spin current with S_z spin polarization, which is advantageous for field-free switching of perpendicular magnetization. Our work may provide unambiguous understanding of the charge and spin transport in noncollinear antiferromagnets and pave the way for applications in antiferromagnetic spintronics.

DOI: 10.1103/PhysRevB.110.054420

I. INTRODUCTION

Noncollinear antiferromagnets (nc-AMFs), such as Mn_3X (X = Ga, Ge, Sn, Pt, Sb, etc.) [1–4] and antiperovskite Mn_3XN (X = Ni, Ga, Sn, etc.) [5–8], etc., have attracted intensive research attention in the field of spintronics. The fascinating transport properties, including anomalous Hall effect (AHE) [9–12], spin-polarized transport [13–15], and tunneling magnetoresistance effect [16–18], make them promising for next-generation spintronic devices, such as magnetic random access memory [19–21].

In recent years, significant advancements have been made in the study of charge and spin Hall effects in nc-AFMs. Notably, the AHE has been theoretically predicted and experimentally observed [9,22–24] in nc-AFMs with vanishing small magnetization, challenging the conventional view that AHE is directly proportional to magnetization in traditional ferromagnets. Furthermore, spin Hall effects have also been theoretically predicted [13,25] even in the absence of spin-orbit coupling and recently observed in Mn_3Sn [14]. Up to now, most of the existing theoretical works on nc-AFMs investigated the individual charge and spin Hall conductivity components [23,25]. In addition, despite the temperature effect having been thoroughly studied in ferromagnets [26,27] and collinear antiferromagnets [28,29], it still remains unclear how temperature may impact the charge and spin transport properties of nc-AFMs, which makes the comparison between experimental and theoretical results unfeasible.

In this work, we leverage linear-response symmetry analysis and tensor transformation relations to gain insights into the fundamental connections between magnetic symmetry, charge, and spin transport in the typical nc-AFM Mn_3Pt. Using first-principles calculations, the specific value of each tensor element for charge and spin Hall conductivity is comprehensively investigated in two representative crystal facet orientations. Furthermore, to more directly compare with experiments, we incorporate lattice vibration and spin disorder scatterings to demonstrate the realistic finite-temperature effect on the charge and spin transport properties in Mn_3Pt.

II. COMPUTATIONAL METHOD

The electronic structure of cubic Mn_3Pt with experimental lattice constant of $a = 3.833$ Å [30] has been calculated self-consistently on the basis of local spin-density approximation (LSDA) as parametrized by Vosko *et al.* [31]. A wave-function expansion with angular momentum cutoff $l_{max} = 3$ is used. To investigate the transport properties, we consider two main temperature-dependent scattering mechanisms, i.e., lattice vibrations (phonon) and spin disorder (spin fluctuation) scattering by employing the coherent phase approximation alloy analogy method implemented in SPR-KKR code [27,32–34], assuming a frozen potential for the atoms [35]. Here, the lattice vibrations are treated by using 14 displacement vectors with the length set to reproduce the temperature-dependent root-mean-square displacement given by Debye's theory [36], where the Debye temperature $\Theta_D = 357$ K estimated from the weighted average of the consisted elements is used. For the spin disorder scattering, we adopt temperature-dependent magnetization $M(T)$ taken from experimental data [37], where the spins are allowed to fluctuate with equal probability on a regular grid of 60 polar angles θ and 5 azimuthal angles φ. The charge and spin Hall conductivity tensors of Mn_3Pt are calculated within the linear-response theory based on

*Contact author: lixinlu@hust.edu.cn
†Contact author: jiazhang@hust.edu.cn

 ©2024 American Physical Society

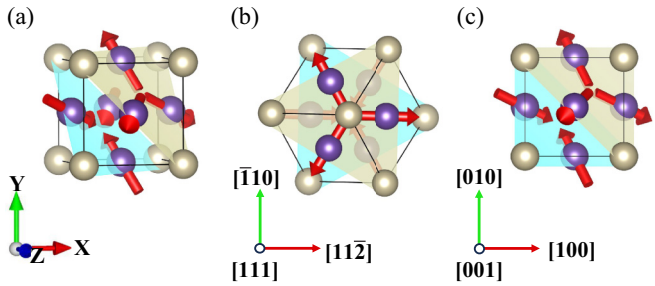

FIG. 1. (a) Crystal structure and spin configuration of cubic nc-AFM Mn_3Pt. (b) and (c) are the top views of Mn_3Pt from (111) and (001) planes. The red, green, and blue arrows along different crystallographic axes indicate the x, y, and z axes in the Cartesian coordinate. (b) and (c) are denoted as config1 and config2, which can be used to study the charge and spin Hall effect for (111) and (001)-oriented Mn_3Pt, respectively.

the Kubo-Středa formula implemented in the Korringa-Kohn-Rostoker Green function method [38–40].

III. RESULTS AND DISCUSSION

A. Symmetry-imposed charge and spin Hall conductivity tensor

The crystal and spin configurations of the typical nc-AFM Mn_3Pt with space group $Pm\bar{3}m$ (No. 221) and magnetic space group $R\bar{3}m$ (No. 166.101) are depicted in Fig. 1(a). We first analyze the symmetry-imposed charge and spin Hall conductivity tensors [41,42]. In linear-response theory, the charge and spin current density propagates along the i direction by applying an electric field $\boldsymbol{E}$, which can be written as

$$J_i = \sum_j \sigma_{ij} E_j \ (i, j \in \{x, y, z\}), \tag{1a}$$

$$J_i^k = \sum_j \sigma_{ij}^k E_j \ (i, j, k \in \{x, y, z\}), \tag{1b}$$

where the charge Hall conductivity σ_{ij} is a tensor of rank 2, and the spin Hall conductivity σ_{ij}^k is a third-rank tensor with k index indicating the spin polarization of the spin current.

The most compact linear-response charge and spin Hall tensors of Mn_3Pt can be obtained in Cartesian coordinate by setting the z axis along [111], x, y along [11$\bar{2}$], and [$\bar{1}$10] crystallographic axes denoted as config1 in Fig. 1(b). This configuration can be adopted for investigating the charge and spin response for (111)-oriented Mn_3Pt film by applying in-plane electric field. The symmetry-imposed charge and spin Hall conductivity tensors for Mn_3Pt (111) in config1 are listed in Table I. Hereafter we use $\tilde{\sigma}$ and $\bar{\sigma}$ to denote the T-odd (time-reversal odd) and T-even (time-reversal even) conductivity tensors. Specifically, the T-odd indicates a sign change of conductivity upon time reversal, while T-even denotes an invariant conductivity by time-reversal operation.

TABLE I. The symmetry-imposed charge and spin conductivity tensors for Mn_3Pt. $\tilde{\sigma}$ and $\bar{\sigma}$ are used to denote the T-odd and T-even conductivity tensors. The charge and spin conductivity in the last column are our calculation results at 0 K with an imaginary energy 10^{-4} Ry. The units for charge Hall conductivity and spin Hall conductivity are in $(\Omega\ \mathrm{cm})^{-1}$ and $(\hbar/2e)(\Omega\ \mathrm{cm})^{-1}$, respectively.

			T-Odd	T-Even	Calculation result
Config1/Mn_3Pt (111)	Charge conductivity	σ	$\begin{pmatrix} 0 & \tilde{\sigma}_{xy} & 0 \\ -\tilde{\sigma}_{xy} & 0 & 0 \\ 0 & 0 & 0 \end{pmatrix}$	$\begin{pmatrix} \bar{\sigma}_{xx} & 0 & 0 \\ 0 & \bar{\sigma}_{xx} & 0 \\ 0 & 0 & \bar{\sigma}_{zz} \end{pmatrix}$	$\begin{pmatrix} 481\,061 & 94 & 0 \\ -94 & 481\,061 & 0 \\ 0 & 0 & 482\,919 \end{pmatrix}$
	Spin conductivity	σ^x	$\begin{pmatrix} \tilde{\sigma}_{xx}^x & 0 & \tilde{\sigma}_{xz}^x \\ 0 & -\tilde{\sigma}_{xx}^x & 0 \\ \tilde{\sigma}_{zx}^x & 0 & 0 \end{pmatrix}$	$\begin{pmatrix} 0 & \bar{\sigma}_{xy}^x & 0 \\ \bar{\sigma}_{xy}^x & 0 & \bar{\sigma}_{yz}^x \\ 0 & \bar{\sigma}_{zy}^x & 0 \end{pmatrix}$	$\begin{pmatrix} -43\,096 & 100 & 72\,062 \\ 100 & 43\,096 & -132 \\ 63\,390 & -176 & 0 \end{pmatrix}$
		σ^y	$\begin{pmatrix} 0 & -\tilde{\sigma}_{xx}^x & 0 \\ -\tilde{\sigma}_{xx}^x & 0 & \tilde{\sigma}_{xz}^x \\ 0 & \tilde{\sigma}_{zx}^x & 0 \end{pmatrix}$	$\begin{pmatrix} \bar{\sigma}_{xy}^x & 0 & -\bar{\sigma}_{yz}^x \\ 0 & -\bar{\sigma}_{xy}^x & 0 \\ -\bar{\sigma}_{zy}^x & 0 & 0 \end{pmatrix}$	$\begin{pmatrix} 100 & 43\,096 & 132 \\ 43\,096 & -100 & 72\,062 \\ 176 & 63\,390 & 0 \end{pmatrix}$
		σ^z	$\begin{pmatrix} \tilde{\sigma}_{xx}^z & 0 & 0 \\ 0 & \tilde{\sigma}_{xx}^z & 0 \\ 0 & 0 & \tilde{\sigma}_{zz}^z \end{pmatrix}$	$\begin{pmatrix} 0 & \bar{\sigma}_{xy}^z & 0 \\ -\bar{\sigma}_{xy}^z & 0 & 0 \\ 0 & 0 & 0 \end{pmatrix}$	$\begin{pmatrix} 4\,602 & 7 & 0 \\ -7 & 4\,602 & 0 \\ 0 & 0 & 4\,497 \end{pmatrix}$
Config2/Mn_3Pt (001)	Charge conductivity	σ	$\begin{pmatrix} 0 & \tilde{\sigma}_{xy} & -\tilde{\sigma}_{xy} \\ -\tilde{\sigma}_{xy} & 0 & \tilde{\sigma}_{xy} \\ \tilde{\sigma}_{xy} & -\tilde{\sigma}_{xy} & 0 \end{pmatrix}$	$\begin{pmatrix} \bar{\sigma}_{xx} & \bar{\sigma}_{xy} & \bar{\sigma}_{xy} \\ \bar{\sigma}_{xy} & \bar{\sigma}_{xx} & \bar{\sigma}_{xy} \\ \bar{\sigma}_{xy} & \bar{\sigma}_{xy} & \bar{\sigma}_{xx} \end{pmatrix}$	$\begin{pmatrix} 481\,681 & 674 & 565 \\ 565 & 481\,681 & 674 \\ 674 & 565 & 481\,681 \end{pmatrix}$
	Spin conductivity	σ^x	$\begin{pmatrix} \tilde{\sigma}_{xx}^x & \tilde{\sigma}_{xy}^x & \tilde{\sigma}_{xy}^x \\ \tilde{\sigma}_{yx}^x & \tilde{\sigma}_{yy}^x & \tilde{\sigma}_{yz}^x \\ \tilde{\sigma}_{yx}^x & \tilde{\sigma}_{yz}^x & \tilde{\sigma}_{yy}^x \end{pmatrix}$	$\begin{pmatrix} 0 & \bar{\sigma}_{xy}^x & -\bar{\sigma}_{xy}^x \\ \bar{\sigma}_{yx}^x & \bar{\sigma}_{yy}^x & \bar{\sigma}_{yz}^x \\ -\bar{\sigma}_{yx}^x & -\bar{\sigma}_{yz}^x & -\bar{\sigma}_{yy}^x \end{pmatrix}$	$\begin{pmatrix} 78\,231 & 3\,684 & 3\,891 \\ -1\,312 & -35\,216 & -2\,613 \\ -1\,125 & -2\,647 & -35\,105 \end{pmatrix}$
		σ^y	$\begin{pmatrix} \tilde{\sigma}_{yy}^x & \tilde{\sigma}_{yx}^x & \tilde{\sigma}_{yz}^x \\ \tilde{\sigma}_{xy}^x & \tilde{\sigma}_{xx}^x & \tilde{\sigma}_{xy}^x \\ \tilde{\sigma}_{yz}^x & \tilde{\sigma}_{yx}^x & \tilde{\sigma}_{yy}^x \end{pmatrix}$	$\begin{pmatrix} -\bar{\sigma}_{yy}^x & -\bar{\sigma}_{yx}^x & -\bar{\sigma}_{yz}^x \\ \bar{\sigma}_{xy}^x & 0 & -\bar{\sigma}_{xy}^x \\ \bar{\sigma}_{yz}^x & \bar{\sigma}_{yx}^x & \bar{\sigma}_{yy}^x \end{pmatrix}$	$\begin{pmatrix} -35\,105 & -1\,125 & -2\,647 \\ 3\,891 & 78\,231 & 3\,684 \\ -2\,613 & -1\,312 & -35\,216 \end{pmatrix}$
		σ^z	$\begin{pmatrix} \tilde{\sigma}_{yy}^x & \tilde{\sigma}_{yz}^x & \tilde{\sigma}_{yx}^x \\ \tilde{\sigma}_{yz}^x & \tilde{\sigma}_{yy}^x & \tilde{\sigma}_{yx}^x \\ \tilde{\sigma}_{xy}^x & \tilde{\sigma}_{xy}^x & \tilde{\sigma}_{xx}^x \end{pmatrix}$	$\begin{pmatrix} \bar{\sigma}_{yy}^x & \bar{\sigma}_{yz}^x & \bar{\sigma}_{yx}^x \\ -\bar{\sigma}_{yz}^x & -\bar{\sigma}_{yy}^x & -\bar{\sigma}_{yx}^x \\ -\bar{\sigma}_{xy}^x & \bar{\sigma}_{xy}^x & 0 \end{pmatrix}$	$\begin{pmatrix} -35\,216 & -2\,613 & -1\,312 \\ -2\,647 & -35\,105 & -1\,125 \\ 3\,684 & 3\,891 & 78\,231 \end{pmatrix}$

As shown in Table I, for Mn_3Pt (111) in config1, the charge Hall conductivity contains only nonzero T-odd term $\tilde{\sigma}_{xy}$. This charge Hall conductivity in nc-AFMs shares the same origin as intrinsic anomalous Hall conductivity in conventional ferromagnetic metals. The T-odd charge Hall conductivity we calculate for Mn_3Pt (111) in config1 at 0 K with a constant band-energy broadening of 10^{-4} Ry is 94 $(\Omega\ \mathrm{cm})^{-1}$, which is comparable to previous theoretical value based on Berry phase method (98 $\Omega^{-1}\ \mathrm{cm}^{-1}$) [23]. For spin Hall effect, each spin conductivity element for Mn_3Pt in config1 contains either a T-odd or T-even term. The T-odd spin Hall conductivity, also known as "magnetic spin Hall," is only present in magnetic materials, while the T-even spin Hall conductivity shares the same origin as nonmagnetic heavy metal like Pt, Ta, etc. [43]. Using the same band-energy broadening, the calculated T-even spin Hall conductivity $\bar{\sigma}^{x}_{xy}$ for Mn_3Pt (111) in config1 at 0 K is 50 $\frac{\hbar}{e}\Omega^{-1}\,\mathrm{cm}^{-1}$, in good agreement with the previous result obtained by Berry phase method [66$(\hbar/e)\ \Omega^{-1}\,\mathrm{cm}^{-1}$] [23]. It is worth noting that for Mn_3Pt (111) in config1, the symmetry-imposed spin Hall conductivity elements $\sigma^{x,y}_{zx}$ and $\sigma^{x,y}_{zy}$ are nonzero but σ^{z}_{zx} and σ^{z}_{zy} are zero, which suggests that the spin current propagates perpendicular to the Mn_3Pt (111) plane by applying in-plane electric field could contain S_x and S_y spin-polarization components, but no out-of-plane S_z component.

The charge and spin Hall conductivity tensors for other crystal facet orientation can be obtained by performing matrix transforming. For instance, by converting from the conductivity tensors for Mn_3Pt (111) in config1 to Mn_3Pt (001) in coordinate system config2 by setting [001] as z axis, [100] as x axis, and [010] as y axis as depicted in Fig. 1(c), the transformation matrix M between those two configurations is as follows:

$$M = \begin{pmatrix} \frac{\sqrt{6}}{6} & -\frac{\sqrt{2}}{2} & \frac{\sqrt{3}}{3} \\ \frac{\sqrt{6}}{6} & \frac{\sqrt{2}}{2} & \frac{\sqrt{3}}{3} \\ -\frac{\sqrt{6}}{3} & 0 & \frac{\sqrt{3}}{3} \end{pmatrix}. \tag{2}$$

The charge conductivity tensors σ_2 for config2 can then be calculated based on σ_1 for config1 by performing the following matrix transformation [24]:

$$\sigma_2 = M\sigma_1 M^{-1}. \tag{3}$$

The symmetry-imposed T-odd and T-even charge conductivity tensors for config2 can be expressed in terms of charge conductivity for config1 as

$$\sigma_2^{(\mathrm{odd})} = \begin{pmatrix} 0 & -\frac{\sqrt{3}}{3}\tilde{\sigma}_{xy} & \frac{\sqrt{3}}{3}\tilde{\sigma}_{xy} \\ \frac{\sqrt{3}}{3}\tilde{\sigma}_{xy} & 0 & -\frac{\sqrt{3}}{3}\tilde{\sigma}_{xy} \\ -\frac{\sqrt{3}}{3}\tilde{\sigma}_{xy} & \frac{\sqrt{3}}{3}\tilde{\sigma}_{xy} & 0 \end{pmatrix}$$

$$\sigma_2^{(\mathrm{even})} = \begin{pmatrix} \frac{2\bar{\sigma}_{xx}+\bar{\sigma}_{zz}}{3} & \frac{\bar{\sigma}_{zz}-\bar{\sigma}_{xx}}{3} & \frac{\bar{\sigma}_{zz}-\bar{\sigma}_{xx}}{3} \\ \frac{\bar{\sigma}_{zz}-\bar{\sigma}_{xx}}{3} & \frac{2\bar{\sigma}_{xx}+\bar{\sigma}_{zz}}{3} & \frac{\bar{\sigma}_{zz}-\bar{\sigma}_{xx}}{3} \\ \frac{\bar{\sigma}_{zz}-\bar{\sigma}_{xx}}{3} & \frac{\bar{\sigma}_{zz}-\bar{\sigma}_{xx}}{3} & \frac{2\bar{\sigma}_{xx}+\bar{\sigma}_{zz}}{3} \end{pmatrix}, \tag{4}$$

where on the right-hand side of the above Eq.(4), $\tilde{\sigma}_{xy}$ is the T-odd charge Hall conductivity, and $\bar{\sigma}_{xx}$ and $\bar{\sigma}_{zz}$ are the anisotropic longitudinal conductivity for Mn_3Pt (111) in config1. It can be seen that in contrast to the sole T-odd Hall conductivity for Mn_3Pt (111), each charge Hall conductivity element for Mn_3Pt (001) comprises both T-odd and T-even contributions. More importantly, the T-even charge Hall conductivity for Mn_3Pt (001) is associated with the anisotropic longitudinal conductivity. Therefore, it will result in a relatively large and highly anisotropic charge Hall conductivity at finite temperature for Mn_3Pt (001), as we will discuss later.

Similarly, the spin Hall conductivity elements for Mn_3Pt (001) in config2 $\sigma^{\ k}_{2,\,ij}$ can be obtained from the spin Hall conductivities for Mn_3Pt (111) in config1 $\sigma^{\ n}_{1,\,lm}$ by the following tensor transformation [24]:

$$\sigma^{\ k}_{2,\,ij} = \sum_{l,m,n} M_{il}M_{jm}M_{kn}\sigma^{\ n}_{1,\,lm}. \tag{5}$$

For instance, the T-odd and T-even spin Hall conductivity elements $\sigma^{x,y,z}_{zx}$ for config2 can be expressed in terms of the spin Hall conductivity for config1 as follows:

$$\begin{aligned}
\sigma_{2,\,zx}^{x(\mathrm{odd})} &= \tfrac{1}{9}\left(\sqrt{6}\tilde{\sigma}^{x}_{xx} - \sqrt{3}\tilde{\sigma}^{z}_{xx} - \sqrt{3}\tilde{\sigma}^{x}_{xz} + 2\sqrt{3}\tilde{\sigma}^{x}_{zx} + \sqrt{3}\tilde{\sigma}^{z}_{zz}\right) \\
\sigma_{2,\,zx}^{y(\mathrm{odd})} &= \tfrac{1}{9}\left(-2\sqrt{6}\tilde{\sigma}^{x}_{xx} - \sqrt{3}\tilde{\sigma}^{z}_{xx} - \sqrt{3}\tilde{\sigma}^{x}_{xz}\right. \\
&\quad \left. - \sqrt{3}\tilde{\sigma}^{x}_{zx} + \sqrt{3}\tilde{\sigma}^{z}_{zz}\right) \\
\sigma_{2,\,zx}^{z(\mathrm{odd})} &= \tfrac{1}{9}\left(\sqrt{6}\tilde{\sigma}^{x}_{xx} - \sqrt{3}\tilde{\sigma}^{z}_{xx} + 2\sqrt{3}\tilde{\sigma}^{x}_{xz} - \sqrt{3}\tilde{\sigma}^{x}_{zx} + \sqrt{3}\tilde{\sigma}^{z}_{zz}\right),
\end{aligned} \tag{6a}$$

$$\begin{aligned}
\sigma_{2,\,zx}^{x(\mathrm{even})} &= \tfrac{1}{3}\left(\sqrt{2}\bar{\sigma}^{y}_{xx} + \bar{\sigma}^{y}_{xz} - \bar{\sigma}^{z}_{yx}\right) \\
\sigma_{2,\,zx}^{y(\mathrm{even})} &= \tfrac{1}{3}\left(-\bar{\sigma}^{y}_{xz} - \bar{\sigma}^{z}_{yx} + \bar{\sigma}^{y}_{zx}\right) \\
\sigma_{2,\,zx}^{z(\mathrm{even})} &= \tfrac{1}{3}\left(-\sqrt{2}\bar{\sigma}^{y}_{xx} - \bar{\sigma}^{z}_{yx} - \bar{\sigma}^{y}_{zx}\right),
\end{aligned} \tag{6b}$$

where the quantities on the right-hand side of the above Eqs. (6a) and (6b) are the corresponding T-odd and T-even spin conductivity elements for config 1. It can be observed from the above equations as well as the symmetry-imposed spin conductivity tensors listed in Table I that all the spin Hall conductivity elements for Mn_3Pt (001) comprise both T-odd and T-even terms. What is more important, $\sigma^{x,y,z}_{zx}$ and $\sigma^{x,y,z}_{zy}$ are all nonzero, which indicates that Mn_3Pt (001) may serve as an efficient spin current source with three spin polarizations (S_x, S_y, and S_z) useful for field-free switching of perpendicular magnetization through spin-orbit torque mechanism. Since Mn_3Pt (111) is relatively trivial (it does not contain T-even charge Hall contribution and there is no spin Hall conductivity for generating S_z spin current), in the following section we will concentrate on the charge and spin transport in Mn_3Pt (001).

B. Charge Hall conductivity of Mn_3Pt: Temperature effects and anisotropy

In order to evaluate the full charge or spin conductivity tensors for nc-AFMs, previous calculations usually adopted constant band-energy broadening (i.e., constant relaxation time) approximation [13]. However, to make a direct comparison between experimental and theoretical results, the finite-temperature effect including phonon and spin disorder scattering should be explicitly taken into account. To better understand the transport property of nc-AFMs at finite temperature, we first calculate and plot the Bloch spectra function

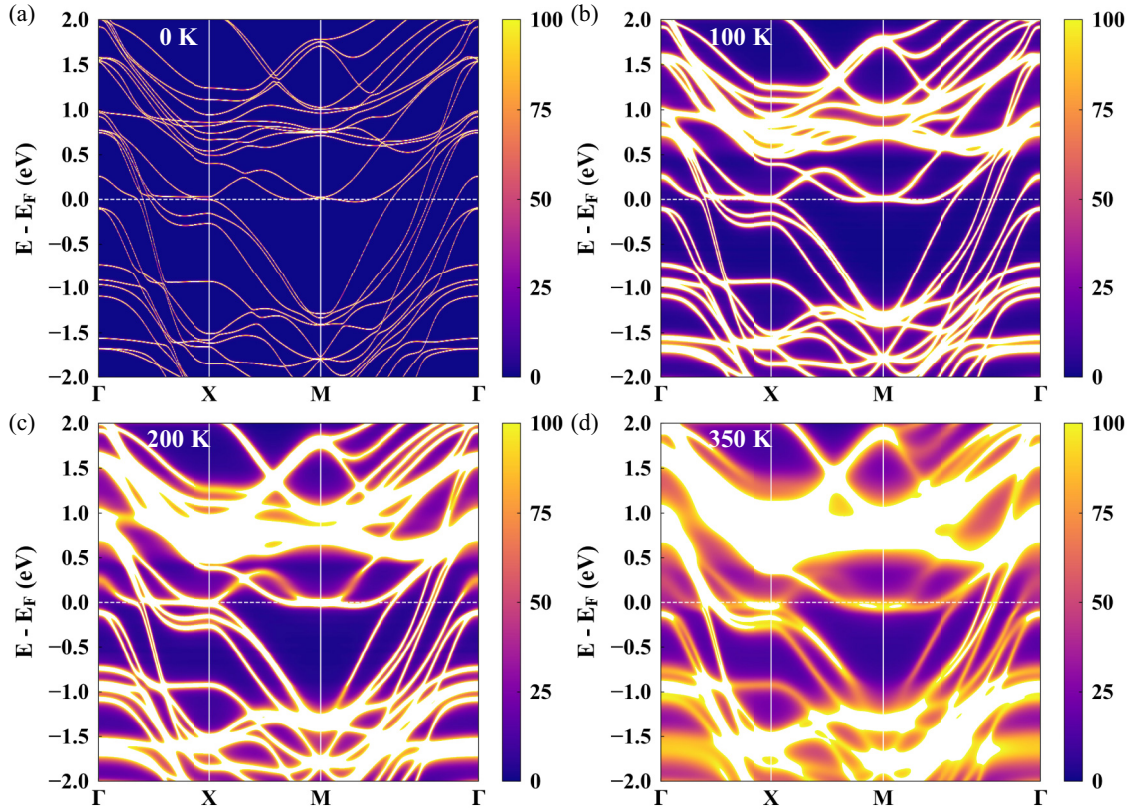

FIG. 2. The Bloch spectra function (BSF) of cubic Mn_3Pt calculated at 0 K (a), 100 K (b), 200 K (c), and 350 K (d). The horizontal white dashed lines indicate the Fermi energy.

(BSF) for cubic Mn_3Pt along the high-symmetry k paths in the Brillouin zone. The calculated BSFs at various temperatures by considering both phonon and spin fluctuation are shown in Fig. 2. At 0 K, the BSF of Mn_3Pt has zero energy broadening (i.e., infinite electron lifetime), which is identical to its band structure shown in Fig. S1 in Supplemental Material [44]. As depicted in Fig. 2(b) to Fig. 2(d), when the temperature is rising, the BSF becomes increasingly blurred. The enhancement of electron scattering with phonon and spin disorder leads to a larger band-energy broadening, and a shorter electron lifetime at higher temperature can also be visible from temperature-dependent density of states shown in Fig. S2 of the Supplemental Material [44].

To have qualitative understanding of general features and temperature dependence of Hall conductivity, we also provide the linear-response formula for conductivity based on Bloch states within the constant band-energy broadening approximation. Under this condition, the T-odd and T-even charge conductivity tensors can be expressed as follows [13,45]:

$$\sigma_{ij}^{(\mathrm{odd})} = e\hbar \sum_{n\neq m} [f(\varepsilon_m) - f(\varepsilon_n)] \frac{\mathrm{Im}(\langle n|\hat{J}_i|m\rangle\langle m|\hat{v}_j|n\rangle)}{(\varepsilon_n - \varepsilon_m)^2 + (\hbar\Gamma)^2}, \quad (7a)$$

$$\sigma_{ij}^{(\mathrm{even})} = -e\hbar^2\Gamma \sum_{n,m} \frac{f(\varepsilon_m) - f(\varepsilon_n)}{\varepsilon_n - \varepsilon_m} \frac{\mathrm{Re}(\langle n|\hat{J}_i|m\rangle\langle m|\hat{v}_j|n\rangle)}{(\varepsilon_n - \varepsilon_m)^2 + (\hbar\Gamma)^2}, \quad (7b)$$

where m and n are the band indices; $f(\varepsilon)$ is the Fermi-Dirac distribution; $\hat{\boldsymbol{J}}$ and $\hat{\boldsymbol{v}}$ represent the electric current density and velocity operators, respectively; e is elementary charge; $\hbar$ is the reduced Planck constant; and $\hbar\Gamma$ is the constant band-energy broadening by taking into account the finite electron lifetime due to scattering.

It is clear that generally the T-odd charge Hall conductivity will decrease with the increase of temperature and band-energy broadening $\hbar\Gamma$. In the clean limit $\Gamma\to 0$, the T-odd charge Hall conductivity $\sigma_{ij}^{(\mathrm{odd})}$ approaches a finite value and restores to Berry phase expression for intrinsic anomalous Hall conductivity [46]. The T-even charge Hall conductivity can be decomposed into intraband ($m = n$) and interband ($m \neq n$) contributions:

$$\sigma_{ij}^{(\mathrm{even,intra})} = \frac{e}{\Gamma} \sum_n \langle n|\hat{J}_i|n\rangle\langle n|\hat{v}_j|n\rangle \left(-\frac{\partial f(\varepsilon_n)}{\partial \varepsilon_n}\right), \quad (8a)$$

$$\sigma_{ij}^{(\mathrm{even,inter})} = -e\hbar^2\Gamma \sum_{n\neq m} \frac{f(\varepsilon_m) - f(\varepsilon_n)}{\varepsilon_n - \varepsilon_m} \times \frac{\mathrm{Re}(\langle n|\hat{J}_i|m\rangle\langle m|\hat{v}_j|n\rangle)}{(\varepsilon_n - \varepsilon_m)^2 + (\hbar\Gamma)^2}. \quad (8b)$$

The T-even charge conductivity including longitudinal conductivity (σ_{ii}) also decreases with the increase of temperature. In the clean limit $\Gamma\to 0$, the interband term $\sigma_{ij}^{(\mathrm{even,inter})}$ gradually vanishes, while the intraband contribution $\sigma_{ij}^{(\mathrm{even,intra})}$ becomes dominating and diverges as a function of $1/\Gamma$.

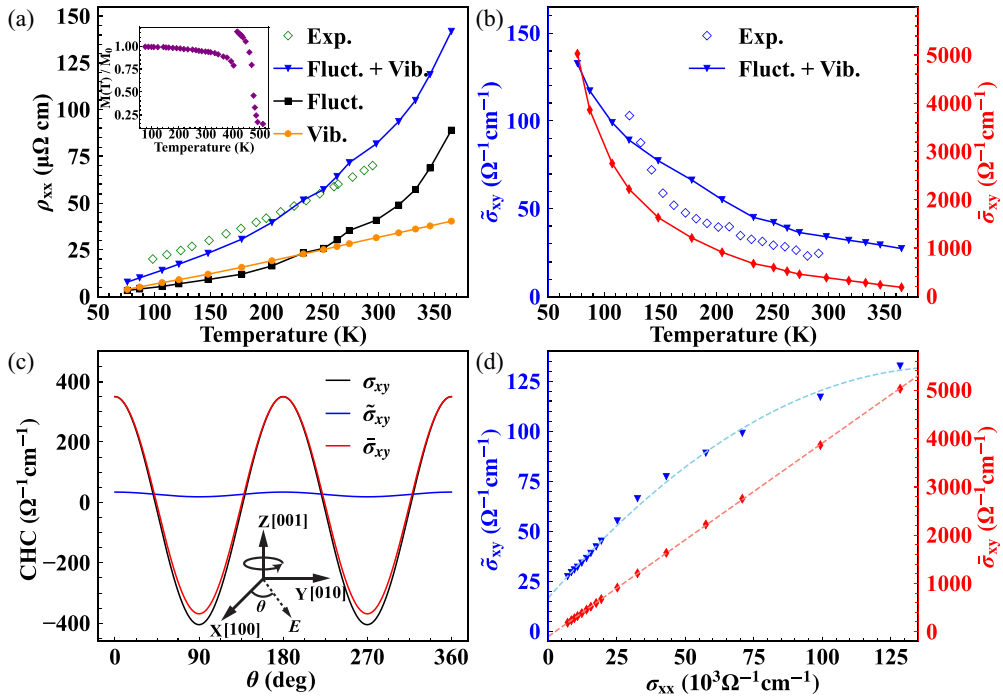

FIG. 3. (a) The calculated temperature dependence of longitudinal resistivity ρ_{xx}. The experimental longitudinal resistivity for single-crystal bulk Mn_3Pt is shown in green open diamond for comparison [47]. The inset is the experimental $M(T)$ curve of Mn_3Pt we use for considering spin-fluctuation scattering. (b) The calculated temperature-dependent T-odd (blue triangles, refer to left axis) and T-even (red diamonds, refer to right axis) charge Hall conductivity of Mn_3Pt (001) in config2. T-odd experimental data are shown in blue open diamonds for comparison [47]. (c) The total T-odd and T-even charge Hall conductivity as a function of θ for Mn_3Pt (001) at room temperature 300 K. The inset shows the definition of angle θ. (d) The calculated T-odd (blue triangles, refer to left axis) and T-even (red diamonds, refer to right axis) charge Hall conductivity as a function of longitudinal conductivity σ_{xx}. The dashed lines are the fitting curves based on scaling relation $\tilde{\sigma}_{xy} \sim a'\sigma_{xx}^2 + b'\sigma_{xx} + c'$ and $\bar{\sigma}_{xy} \sim a\sigma_{xx} + b$, respectively.

We then calculate the temperature-dependent charge conductivity by including phonon and spin disorder scatterings by using an alloy analogy model as implemented in Green's function-based spin-polarized relativistic Korringa-Kohn-Rostoker (SPR-KKR) method [33]. We first compare the longitudinal resistivity ρ_{xx} with the available experimental results for bulk single-crystal Mn_3Pt [47]. As shown in Fig. 3(a), the calculated electrical resistivity by considering both lattice vibration and spin fluctuation agrees well with the experimental result. When only the lattice vibration effect is included, the phonon resistivity ρ_{xx}^{vib} scales almost linearly with temperature T. In the low-temperature regime ($T <$ 200 K), the spin-fluctuation resistivity ρ_{xx}^{flu} is comparable to ρ_{xx}^{vib}, and ρ_{xx}^{flu} is dominant over ρ_{xx}^{vib} in the high-temperature regime ($T >$ 220 K), which indicates that the spin disorder scattering in nc-AFMs is vital for charge and spin transport at finite temperatures.

Experimentally, the anomalous Hall resistivity of nc-AFMs has usually been measured and evaluated by $\frac{1}{2}[\rho_{xy}^{+}(H=0) - \rho_{xy}^{-}(H=0)]$, which only contains the T-odd term, where $\rho_{xy}^{\pm}(H=0)$ refer to Hall resistivity measured at zero magnetic field after applying opposite magnetic field [10,47]. It is worth noting that when thermal scatterings including phonon and spin disorder have been considered, the shape of Hall conductivity tensors may deviate from the zero-temperature case as outlined in Table I. However, in our first-principles calculation, all the conductivity tensors have been explicitly calculated, instead of deduced from symmetry restrictions. The T-even and T-odd contributions have been distinguished and obtained by performing two separate calculations for Mn_3Pt with opposite spin configurations by $\sigma_H^{\text{odd}} = \frac{1}{2}[\sigma_H(\boldsymbol{M}) - \sigma_H(-\boldsymbol{M})]$ and $\sigma_H^{\text{even}} = \frac{1}{2}[\sigma_H(\boldsymbol{M}) + \sigma_H(-\boldsymbol{M})]$, where $\boldsymbol{M}$ and $-\boldsymbol{M}$ denote the opposite spin configurations in Mn_3Pt. As shown in Fig. 3(b), the calculated T-odd charge Hall conductivity for Mn_3Pt (001) agrees well with the experimental result in a wide temperature window. At room temperature ($T = 300$ K), the calculated T-odd Hall conductivity is 33 $(\Omega\ \text{cm})^{-1}$, which is close to the experimental value of 25 $(\Omega\ \text{cm})^{-1}$ [47].

As shown in Fig. 3(b), both calculated T-odd and T-even charge Hall conductivity decrease with increasing temperature. At the same temperature, the T-even charge Hall conductivity $\bar{\sigma}_{xy}$, which is associated with the anisotropic longitudinal transport, is dozens of times larger than the T-odd charge Hall conductivity $\tilde{\sigma}_{xy}$. We further investigate the scaling relation between charge Hall conductivity and longitudinal conductivity σ_{xx}. As shown in Fig. 3(d), the T-even charge Hall conductivity $\bar{\sigma}_{xy}$ can be well described by linearly scaling with σ_{xx} as $\bar{\sigma}_{xy} \sim a\sigma_{xx} + b$, since the T-even conductivity shows the similar dependence on band-energy broadening as indicated in Eq. (7). However, the T-odd charge Hall conductivity $\tilde{\sigma}_{xy}$, which exhibits different dependence on band-energy broadening, should be described by including

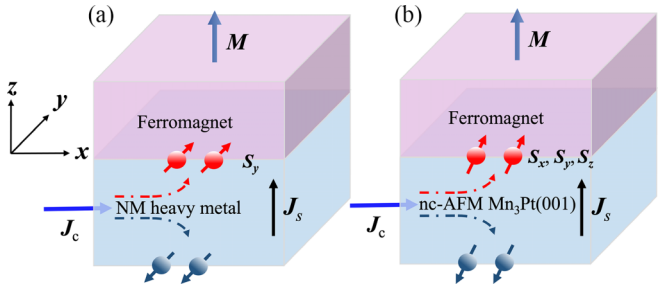

FIG. 4. Comparison of spin Hall effect for SOT applications: (a) Conventional nonmagnetic heavy metals like Pt and Ta may generate spin current along z direction with only S_y spin polarization by applying charge current J_c along x direction. (b) Representative nc-AFM such as Mn_3Pt (001) could produce spin current with all three spin polarizations S_x, S_y, and S_z, which is beneficial for field-free switching of perpendicular magnetization.

both linear and quadratic scaling with σ_{xx} as $\tilde{\sigma}_{xy} \sim a'\sigma_{xx}^2 + b'\sigma_{xx} + c'$. Such scaling relation between $\tilde{\sigma}_{xy}$ and σ_{xx} for Mn_3Pt film has been reported by recent experiment [48].

The in-plane anisotropy of charge Hall conductivity for Mn_3Pt (001) at room temperature is further studied. As shown in Fig. 3(c), θ has been set to be the angle between electric field and the [100] crystal axis. By employing similar matrix transformation as shown in Eq. (3), the charge Hall conductivity for Mn_3Pt (001) with arbitrary in-plane angle θ with respect to config2 can be obtained by the following transformation matrix:

$$M = \begin{pmatrix} \cos\theta & -\sin\theta & 0 \\ \sin\theta & \cos\theta & 0 \\ 0 & 0 & 1 \end{pmatrix}. \tag{9}$$

The calculated total charge Hall conductivity σ_{xy}, the T-odd ($\tilde{\sigma}_{xy}$), and T-even ($\bar{\sigma}_{xy}$) Hall conductivity as a function of θ are shown in Fig 3(c). The anisotropic charge Hall conductivity generally follows a sinusoidal function with a π periodicity. The highly anisotropic total Hall conductivity σ_{xy} can be attributed to the dominant T-even Hall conductivity $\bar{\sigma}_{xy}$. The T-even charge Hall conductivity reaches its maximum value 350 Ω^{-1} cm^{-1} at $\theta = 0$, an order of magnitude larger than the T-odd Hall conductivity (34 Ω^{-1}cm^{-1}).

C. Spin Hall conductivity of Mn_3Pt: Temperature effects and anisotropy

The spin current generated by spin Hall effect with out-of-plane S_z component (spin-polarization perpendicular to film plane) is essential for field-free switching of perpendicular magnetization. However, as shown in Fig. 4(a), in conventional nonmagnetic heavy metal like Pt and Ta, the spin current propagating perpendicular to the film plane only has in-plane spin polarization when in-plane charge current is applied. Recently, several experiments demonstrated that nc-AFMs can generate spin current with three spin polarizations (S_x, S_y, S_z), which makes nc-AFMs an appealing spin current source for spin-orbit torque (SOT) applications [20,21]. The full spin conductivity tensor for Mn_3Pt (001) in config2 can be found in Table I. It can be seen that all spin Hall conductivity elements, especially $\sigma_{zx}^{x,y,z}$ and $\sigma_{zy}^{x,y,z}$ are nonzero and contributed by major T-odd and minor T-even terms. This indicates that as shown in Fig. 4(b) for Mn_3Pt (001) film, there will be spin current with three spin-polarization components (S_x, S_y, S_z) propagating along the z direction by applying an in-plane electric field, which makes Mn_3Pt (001) and similar nc-AFMs promising spin current sources for SOT application.

Similar to charge conductivity, the linear-response T-odd and T-even spin conductivity based on constant band-energy broadening approximation can be obtained by replacing charge current-density operator with spin current operator $\hat{J}_i^k = \frac{1}{2}\{\hat{s}_k, \hat{v}_i\}$ and interchange T-odd and T-even terms in Eq. (7) as [13,45]

$$\sigma_{ij}^{k(\text{even})} = e\hbar \sum_{n\neq m} [f(\varepsilon_m) - f(\varepsilon_n)] \frac{\text{Im}\left(\langle n|\hat{J}_i^k|m\rangle\langle m|\hat{v}_j|n\rangle\right)}{(\varepsilon_n - \varepsilon_m)^2 + (\hbar\Gamma)^2}, \tag{10a}$$

$$\sigma_{ij}^{k(\text{odd})} = -e\hbar^2\Gamma \sum_{n,m} \frac{f(\varepsilon_m) - f(\varepsilon_n)}{\varepsilon_n - \varepsilon_m} \frac{\text{Re}\left(\langle n|\hat{J}_i^k|m\rangle\langle m|\hat{v}_j|n\rangle\right)}{(\varepsilon_n - \varepsilon_m)^2 + (\hbar\Gamma)^2}, \tag{10b}$$

It is clear that generally the T-even spin Hall conductivity $\sigma_{ij}^{k(\text{even})}$ decreases with the increase of temperature. In the clean limit $\Gamma \to 0$, the T-even spin Hall conductivity approaches a finite value and can be evaluated based on Berry phase expression for intrinsic spin Hall conductivity [49]. The T-odd spin Hall conductivity (i.e., magnetic spin Hall conductivity) $\sigma_{ij}^{k(\text{odd})}$ can be decomposed into intraband ($m = n$) and interband ($m \neq n$) contributions:

$$\sigma_{ij}^{k(\text{odd,intra})} = \frac{e}{\Gamma} \sum_n \langle n|\hat{J}_i^k|n\rangle\langle n|\hat{v}_j|n\rangle \left(-\frac{\partial f(\varepsilon_n)}{\partial \varepsilon_n}\right), \tag{11a}$$

$$\sigma_{ij}^{k(\text{odd,inter})} = -e\hbar^2\Gamma \sum_{n\neq m} \frac{f(\varepsilon_m) - f(\varepsilon_n)}{\varepsilon_n - \varepsilon_m} \times \frac{\text{Re}(\langle n|\hat{J}_i^k|m\rangle\langle m|\hat{v}_j|n\rangle)}{(\varepsilon_n - \varepsilon_m)^2 + (\hbar\Gamma)^2}. \tag{11b}$$

The T-odd spin Hall conductivity also decreases when the temperature increases. In the clean limit $\Gamma \to 0$, the interband term $\sigma_{ij}^{k(\text{odd,inter})}$ gradually reduces to zero, while the intraband contribution $\sigma_{ij}^{k(\text{odd,intra})}$ becomes dominating and diverges as a function of $1/\Gamma$.

We then calculate the temperature-dependent spin Hall conductivity (SHC) by including both phonon and spin disorder scatterings. It can be seen from Table I that the spin Hall conductivity elements for Mn_3Pt (001) in config2 are mostly contributed by the T-odd term, with a small portion of T-even term. Figures 5(a) to Fig. 5(c) present the temperature dependency of three typical spin Hall conductivity elements σ_{zx}^x, σ_{zx}^y, and σ_{zx}^z for Mn_3Pt (001). At low temperature, the SHCs are all at the order of $10^3\hbar/2e(\Omega\,\text{cm})^{-1}$. With the increase of temperature, the absolute values of all three SHCs drastically decrease and drop to around $10^2\hbar/2e(\Omega\,\text{cm})^{-1}$ at room temperature, 300 K.

The scaling relation between spin Hall conductivity with longitudinal conductivity σ_{xx} has also been investigated. As it is shown in Figs. 5(d)–5(g), all three spin Hall conductivity

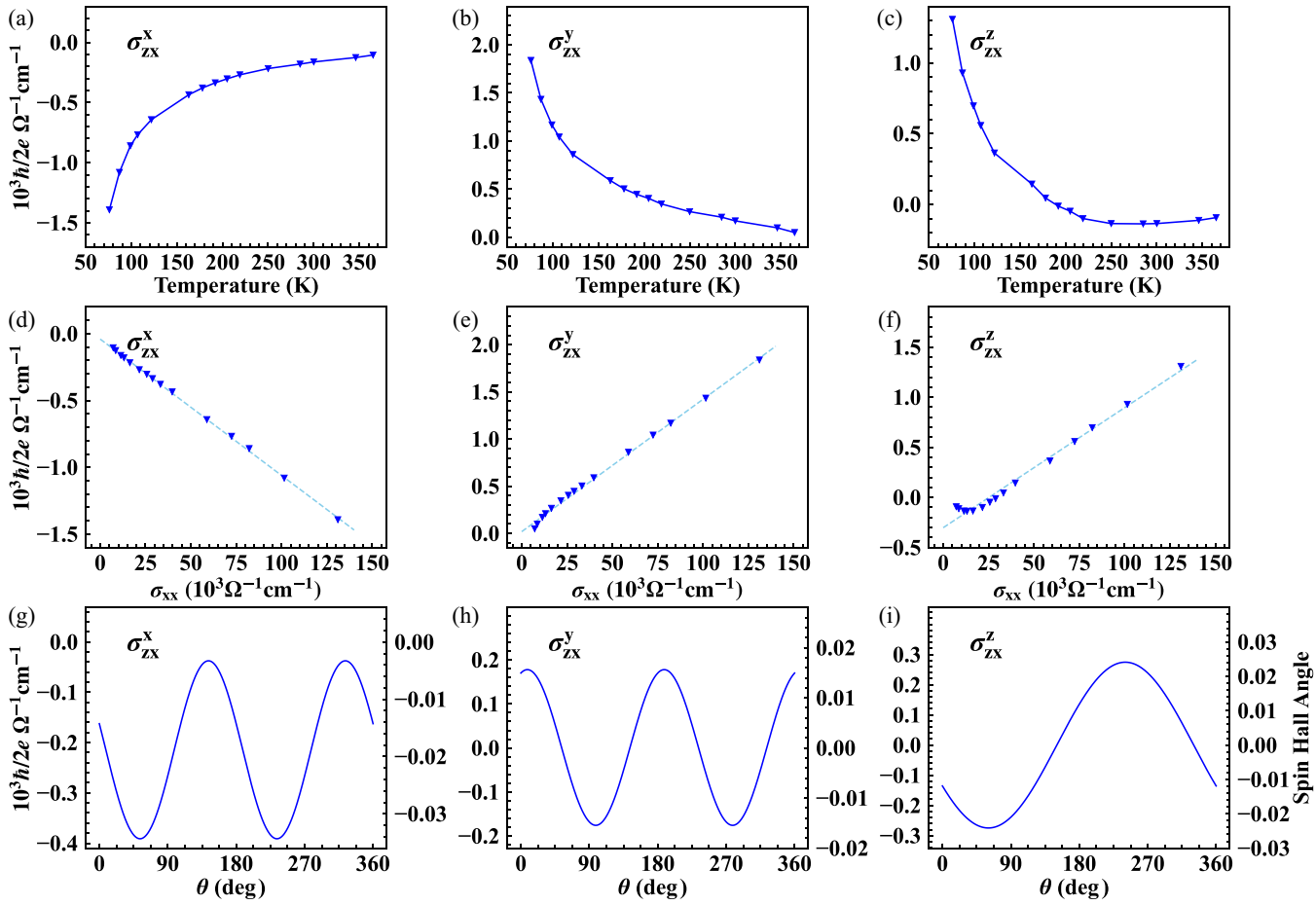

FIG. 5. The calculated spin Hall conductivity σ_{zx}^{x} (a), σ_{zx}^{y} (b), and σ_{zx}^{z} (c) of Mn_3Pt (001) in config2 as a function of temperature. (d)–(f) are the scaling relation between σ_{zx}^{x}, σ_{zx}^{y}, and σ_{zx}^{z} and the longitudinal conductivity σ_{xx}, where the dashed lines are linear fittings by $\sigma_{zx}^{x,y,z} \sim a\sigma_{xx} + b$. (g)–(i) are the in-plane anisotropic spin Hall conductivity (refer to left axis) and the corresponding spin Hall angle (refer to right axis) for Mn_3Pt (001) at room temperature (300 K).

elements $\sigma_{zx}^{x,y,z}$ follow linear scaling with σ_{xx} and can be well described as $\sigma_{zx}^{k} \sim a\sigma_{xx} + b$. Such linear scaling behavior of spin Hall conductivity can be understood based on the fact that both the dominating T-odd spin Hall conductivity and the T-even longitudinal conductivity σ_{xx} exhibit similar dependence on band-energy broadening $\hbar\Gamma$ as indicated in Eq. (10b) and Eq. (7b).

The arbitrary in-plane angle θ dependence of $\sigma_{zx}^{x,y,z}(\theta)$ for Mn_3Pt (001) can be obtained from spin Hall tensor of Mn_3Pt (001) in config2 by performing tensor transformation by following Eq. (6):

$$\begin{aligned}
\sigma_{zx}^{x}(\theta) &= \sigma_{zx}^{x}\cos^2\theta - \frac{\sigma_{zx}^{y}\sin 2\theta}{2} - \frac{\sigma_{zy}^{x}\sin 2\theta}{2} + \sigma_{zy}^{y}\sin^2\theta,\\
\sigma_{zx}^{y}(\theta) &= \frac{\sigma_{zx}^{x}\sin 2\theta}{2} + \sigma_{zx}^{y}\cos^2\theta - \sigma_{zy}^{x}\sin^2\theta - \frac{\sigma_{zy}^{y}\sin 2\theta}{2},\\
\sigma_{zx}^{z}(\theta) &= \sigma_{zx}^{z}\cos\theta - \sigma_{zy}^{z}\sin\theta, \qquad (12)
\end{aligned}$$

where on the right-hand side are the corresponding spin Hall conductivities for Mn_3Pt (001). The calculated spin Hall conductivities and corresponding spin Hall angles $\alpha^{x,y,z}$ [the spin Hall angles are defined as $\alpha^{x,y,z} = \frac{2e}{\hbar}(\frac{\sigma_{zx}^{x,y,z}}{\sigma_{xx}})$] as functions of in-plane angle θ at room temperature are shown in Fig. 5(g) to Fig. 5(i). It can be seen that $\alpha^{x,y,z}$ are all of the order of several percent. $\alpha^{x,y}(\theta)$ follow a π periodicity, while $\alpha^{z}(\theta)$ has a 2π periodicity as manifested in Eq. (12).

We then focus on α^{z} and σ_{zx}^{z}, which are essential for field-free switching of perpendicular magnetization. The peak spin Hall angle α^{z} for (001)-oriented Mn_3Pt is calculated to be 0.024, corresponding to spin Hall conductivity $\sigma_{zx}^{z} = 275\hbar/2e\Omega^{-1}$ cm^{-1}. As illustrated in Fig. 6, the calculated spin Hall conductivity σ_{zx}^{z} of Mn_3Pt (001) for S_z spin polarization is the largest among the available materials and of the same order as Mn_3Ir ($143\hbar/2e\Omega^{-1}$ cm^{-1}) [50] and 2D $WTe_2/PtTe_2$ heterostructure ($250\hbar/2e\Omega^{-1}$ cm^{-1}) [51]. Therefore, spin current with large S_z spin polarization can be generated by spin Hall effect in Mn_3Pt (001), which is particularly advantageous for spin-orbit torque (SOT) applications.

IV. SUMMARY

In summary, we have presented first-principles calculations for the charge and spin Hall effects in nc-AFM Mn_3Pt at finite temperature by including phonon and spin disorder scatterings. The charge and spin transports are found to be critically dependent on crystal facet orientation. For Mn_3Pt (001) it contains both T-odd and T-even charge Hall contribution, while the T-even part is associated with anisotropic longitudinal

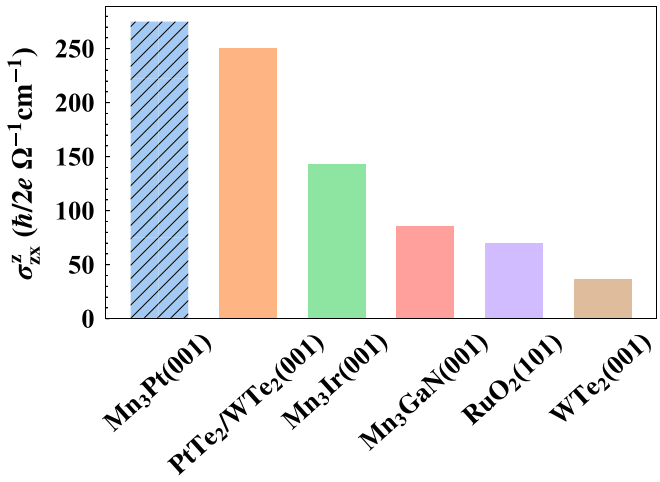

FIG. 6. Comparison of the calculated spin Hall conductivity σ^z_{zx} relevant for spin current with out-of-plane S_z spin polarization for Mn_3Pt (001) at 300 K and the reported experimental results for $PtTe_2/WTe_2/$ [51], Mn_3Ir [50], Mn_3GaN [52], RuO_2 [53], and WTe_2 [54].

transport, leading to relatively large and highly anisotropic total Hall conductivity. The T-even charge Hall conductivity shows linear scaling with longitudinal conductivity σ_{xx}, while the T-odd term should be scaled by also including a quadratic term. The spin Hall conductivity tensors for Mn_3Pt (001) are full and each element comprises major T-odd contribution and minor T-even contribution, making spin Hall conductivity linearly scaling with σ_{xx}. The large spin Hall conductivity element for producing out-of-plane spin-polarization S_z at room temperature makes it useful for field-free switching of perpendicular magnetization in SOT applications. Notably, our findings on Mn_3Pt can be naturally extended to a broad family of other nc-AFMs with similar magnetic structures, such as Mn_3Ir, Mn_3Rh, Mn_3Sb, and their alloys. Our work may provide comprehensive understanding of the charge and spin Hall effect in nc-AFMs and pave the way for potential applications in spintronic devices.

ACKNOWLEDGMENTS

This work was supported by the National Natural Science Foundation of China (Grants No. T2394475 and No. T2394470), and the open research fund of Beijing National Laboratory for Condensed Matter Physics (Grant No. 2023BNLCMPKF010). Xinlu Li was supported by the China Postdoctoral Science Foundation under Grant No. 2023M741269.

[1] H. Hayashi, Y. Shirako, L. Xing, A. A. Belik, M. Arai, M. Kohno, T. Terashima, H. Kojitani, M. Akaogi, and K. Yamaura, Large anomalous Hall effect observed in the cubic-lattice antiferromagnet Mn_3Sb with kagome lattice, Phys. Rev. B **108**, 075140 (2023).

[2] S. Khmelevskyi, A. V. Ruban, and P. Mohn, Magnetic ordering and exchange interactions in structural modifications of Mn_3Ga alloys: Interplay of frustration, atomic order, and off-stoichiometry, Phys. Rev. B **93**, 184404 (2016).

[3] M. Ikhlas, S. Dasgupta, F. Theuss, T. Higo, S. Kittaka, B. J. Ramshaw, O. Tchernyshyov, C. W. Hicks, and S. Nakatsuji, Piezomagnetic switching of the anomalous Hall effect in an antiferromagnet at room temperature, Nat. Phys. **18**, 1086 (2022).

[4] P. Taivansaikhan and D. Odkhuu, Tailorable magnetocrystalline anisotropy at the $MnPt_3$ (001) surface, Phys. Rev. B **106**, 104413 (2022).

[5] B. H. Rimmler, B. K. Hazra, B. Pal, K. Mohseni, J. M. Taylor, A. Bedoya-Pinto, H. Deniz, M. Tangi, I. Kostanovskiy, C. Luo *et al.*, Atomic displacements enabling the observation of the anomalous Hall effect in a non-collinear antiferromagnet, Adv. Mater. **35**, 2209616 (2023).

[6] G. Gurung, D.-F. Shao, T. R. Paudel, and E. Y. Tsymbal, Anomalous Hall conductivity of noncollinear magnetic antiperovskites, Phys. Rev. Mater. **3**, 044409 (2019).

[7] G. Gurung, D.-F. Shao, and E. Y. Tsymbal, Transport spin polarization of noncollinear antiferromagnetic antiperovskites, Phys. Rev. Mater. **5**, 124411 (2021).

[8] X. Zhou, J.-P. Hanke, W. Feng, F. Li, G.-Y. Guo, Y. Yao, S. Blügel, and Y. Mokrousov, Spin-order dependent anomalous Hall effect and magneto-optical effect in the noncollinear antiferromagnets Mn_3XN with X = Ga, Zn, Ag, or Ni, Phys. Rev. B **99**, 104428 (2019).

[9] H. Chen, Q. Niu, and A. H. MacDonald, Anomalous Hall effect arising from noncollinear antiferromagnetism, Phys. Rev. Lett. **112**, 017205 (2014).

[10] Z. Q. Liu, H. Chen, J. M. Wang, J. H. Liu, K. Wang, Z. X. Feng, H. Yan, X. R. Wang, C. B. Jiang, J. M. D. Coey *et al.*, Electrical switching of the topological anomalous Hall effect in a non-collinear antiferromagnet above room temperature, Nat. Electron. **1**, 172 (2018).

[11] H. Iwaki, M. Kimata, T. Ikebuchi, Y. Kobayashi, K. Oda, Y. Shiota, T. Ono, and T. Moriyama, Large anomalous Hall effect in $L1_2$-ordered antiferromagnetic Mn_3Ir thin films, Appl. Phys. Lett. **116**, 022408 (2020).

[12] J. Mukherjee, T. S. Suraj, H. Basumatary, K. Sethupathi, and K. V. Raman, Sign reversal of anomalous Hall conductivity and magnetoresistance in cubic noncollinear antiferromagnet Mn_3Pt thin films, Phys. Rev. Mater. **5**, 014201 (2021).

[13] J. Železný, Y. Zhang, C. Felser, and B. Yan, Spin-polarized current in noncollinear antiferromagnets, Phys. Rev. Lett. **119**, 187204 (2017).

[14] M. Kimata, H. Chen, K. Kondou, S. Sugimoto, P. K. Muduli, M. Ikhlas, Y. Omori, T. Tomita, A. H. MacDonald, S. Nakatsuji *et al.*, Magnetic and magnetic inverse spin Hall effects in a non-collinear antiferromagnet, Nature (London) **565**, 627 (2019).

[15] K. Kondou, H. Chen, T. Tomita, M. Ikhlas, T. Higo, A. H. MacDonald, S. Nakatsuji, and Y. Otani, Giant field-like torque by the out-of-plane magnetic spin Hall effect in a topological antiferromagnet, Nat. Commun. **12**, 1 (2021).

[16] J. Dong, X. Li, G. Gurung, M. Zhu, P. Zhang, F. Zheng, E. Y. Tsymbal, and J. Zhang, Tunneling magnetoresistance in noncollinear antiferromagnetic tunnel junctions, Phys. Rev. Lett. **128**, 197201 (2022).

[17] P. Qin, H. Yan, X. Wang, H. Chen, Z. Meng, J. Dong, M. Zhu, J. Cai, Z. Feng, X. Zhou *et al.*, Room-temperature magnetoresistance in an all-antiferromagnetic tunnel junction, Nature (London) **613**, 485 (2023).

[18] X. Chen, T. Higo, K. Tanaka, T. Nomoto, H. Tsai, H. Idzuchi, M. Shiga, S. Sakamoto, R. Ando, H. Kosaki *et al.*, Octupole-driven magnetoresistance in an antiferromagnetic tunnel junction, Nature (London) **613**, 490 (2023).

[19] D. Xiong, Y. Jiang, K. Shi, A. Du, Y. Yao, Z. Guo, D. Zhu, K. Cao, S. Peng, W. Cai *et al.*, Antiferromagnetic spintronics: An overview and outlook, Fundam. Res. **2**, 522 (2022).

[20] S. Hu, D.-F. Shao, H. Yang, C. Pan, Z. Fu, M. Tang, Y. Yang, W. Fan, S. Zhou, E. Y. Tsymbal *et al.*, Efficient perpendicular magnetization switching by a magnetic spin Hall effect in a noncollinear antiferromagnet, Nat. Commun. **13**, 4447 (2022).

[21] C. Cao, S. Chen, R.-C. Xiao, Z. Zhu, G. Yu, Y. Wang, X. Qiu, L. Liu, T. Zhao, D.-F. Shao *et al.*, Anomalous spin current anisotropy in a noncollinear antiferromagnet, Nat. Commun. **14**, 5873 (2023).

[22] J. Kübler and C. Felser, Non-collinear antiferromagnets and the anomalous Hall effect, EPL **108**, 67001 (2014).

[23] Y. Zhang, Y. Sun, H. Yang, J. Železný, S. P. P. Parkin, C. Felser, and B. Yan, Strong anisotropic anomalous Hall effect and spin Hall effect in the chiral antiferromagnetic compounds Mn_3X (X = Ge, Sn, Ga, Ir, Rh, and Pt), Phys. Rev. B **95**, 075128 (2017).

[24] W. Zhang, W. Han, S.-H. Yang, Y. Sun, Y. Zhang, B. Yan, and S. S. P. Parkin, Giant facet-dependent spin-orbit torque and spin Hall conductivity in the triangular antiferromagnet $IrMn_3$, Sci. Adv. **2**, e1600759 (2016).

[25] Y. Zhang, J. Železný, Y. Sun, J. van den Brink, and B. Yan, Spin Hall effect emerging from a noncollinear magnetic lattice without spin–orbit coupling, New J. Phys. **20**, 073028 (2018).

[26] J. Banhart and H. Ebert, First-principles theory of spontaneous-resistance anisotropy and spontaneous Hall effect in disordered ferromagnetic alloys, Europhys. Lett. **32**, 517 (1995).

[27] K. Chadova, S. Mankovsky, J. Minár, and H. Ebert, Impact of finite temperatures on the transport properties of Gd from first principles, Phys. Rev. B **95**, 125109 (2017).

[28] D. Wagenknecht, K. Výborný, K. Carva, and I. Turek, Antiferromagnetic CuMnAs: *Ab initio* description of finite temperature magnetism and resistivity, J. Magn. Magn. Mater. **513**, 167078 (2020).

[29] S. Mankovsky, S. Polesya, K. Chadova, H. Ebert, J. B. Staunton, T. Gruenbaum, M. A. W. Schoen, C. H. Back, X. Z. Chen, and C. Song, Temperature-dependent transport properties of FeRh, Phys. Rev. B **95**, 155139 (2017).

[30] E. Krén, G. Kádár, L. Pál, J. Sólyom, P. Szabó, and T. Tarnóczi, Magnetic structures and exchange interactions in the Mn-Pt system, Phys. Rev. **171**, 574 (1968).

[31] S. H. Vosko, L. Wilk, and M. Nusair, Accurate spin-dependent electron liquid correlation energies for local spin density calculations: A critical analysis, Can. J. Phys. **58**, 1200 (1980).

[32] J. S. Faulkner and G. M. Stocks, Calculating properties with the coherent-potential approximation, Phys. Rev. B **21**, 3222 (1980).

[33] H. Ebert, S. Mankovsky, K. Chadova, S. Polesya, J. Minár, and D. Ködderitzsch, Calculating linear-response functions for finite temperatures on the basis of the alloy analogy model, Phys. Rev. B **91**, 165132 (2015).

[34] D. Ködderitzsch, K. Chadova, J. Minár, and H. Ebert, Impact of finite temperatures and correlations on the anomalous Hall conductivity from *ab initio* theory, New J. Phys. **15**, 053009 (2013).

[35] J. K. Glasbrenner, K. D. Belashchenko, J. Kudrnovský, V. Drchal, S. Khmelevskyi, and I. Turek, First-principles study of spin-disorder resistivity of heavy rare-earth metals: Gd-Tm series, Phys. Rev. B **85**, 214405 (2012).

[36] O. Šipr, S. Wimmer, S. Mankovsky, and H. Ebert, Transport properties of doped permalloy via *ab initio* calculations: Effect of host disorder, Phys. Rev. B **101**, 085109 (2020).

[37] H. Yasui, M. Ohashi, S. Abe, H. Yoshida, T. Kaneko, Y. Yamaguchi, and T. Suzuki, Magnetic order-order transformation in Mn_3Pt, J. Magn. Magn. Mater. **104**, 927 (1992).

[38] H. Ebert, J. Braun, D. Ködderitzsch, and S. Mankovsky, Fully relativistic multiple scattering calculations for general potentials, Phys. Rev. B **93**, 075145 (2016).

[39] D. Ködderitzsch, S. Lowitzer, J. B. Staunton, and H. Ebert, Electronic and transport properties of disordered transition-metal alloys, Phys. Status Solidi B **248**, 2248 (2011).

[40] S. Lowitzer, D. Ködderitzsch, and H. Ebert, Coherent description of the intrinsic and extrinsic anomalous Hall effect in disordered alloys on an *ab initio* level, Phys. Rev. Lett. **105**, 266604 (2010).

[41] H. T. Stokes and D. M. Hatch, *FINDSYM:* Program for identifying the space-group symmetry of a crystal, J. Appl. Crystallogr. **38**, 237 (2005).

[42] J. Železný, H. Gao, A. Manchon, F. Freimuth, Y. Mokrousov, J. Zemen, J. Mašek, J. Sinova, and T. Jungwirth, Spin-orbit torques in locally and globally noncentrosymmetric crystals: Antiferromagnets and ferromagnets, Phys. Rev. B **95**, 014403 (2017).

[43] G. Y. Guo, S. Murakami, T.-W. Chen, and N. Nagaosa, Intrinsic spin Hall effect in platinum: First-principles calculations, Phys. Rev. Lett. **100**, 096401 (2008).

[44] See Supplemental Material at http://link.aps.org/supplemental/10.1103/PhysRevB.110.054420 for band structure and density of states (DOS) of Mn_3Pt.

[45] A. Crépieux and P. Bruno, Theory of the anomalous Hall effect from the Kubo formula and the Dirac equation, Phys. Rev. B **64**, 014416 (2001).

[46] N. Nagaosa, J. Sinova, S. Onoda, A. H. MacDonald, and N. P. Ong, Anomalous Hall effect, Rev. Mod. Phys. **82**, 1539 (2010).

[47] B. E. Zuniga-Cespedes, K. Manna, H. M. L. Noad, P.-Y. Yang, M. Nicklas, C. Felser, A. P. Mackenzie, and C. W. Hicks, Observation of an anomalous Hall effect in single-crystal Mn_3Pt, New J. Phys. **25**, 023029 (2023).

[48] S. Xu, B. Dai, Y. Jiang, D. Xiong, H. Cheng, L. Tai, M. Tang, Y. Sun, Y. He, B. Yang *et al.*, Universal scaling law for chiral antiferromagnetism, Nat. Commun. **15**, 3717 (2024).

[49] J. Sinova, S. O. Valenzuela, J. Wunderlich, C. H. Back, and T. Jungwirth, Spin Hall effects, Rev. Mod. Phys. **87**, 1213 (2015).

[50] Y. Pu, G. Shi, Q. Yang, D. Yang, F. Wang, C. Zhang, and H. Yang, Field-free switching of perpendicular magnetization by anisotropic spin Hall effect in Mn_3Ir, Adv. Funct. Mater. 2400143 (2024).

[51] F. Wang, G. Shi, K.-W. Kim, H.-J. Park, J. G. Jang, H. R. Tan, M. Lin, Y. Liu, T. Kim, D. Yang *et al.*, Field-free switching of perpendicular magnetization by two-dimensional $PtTe_2/WTe_2$ van der Waals heterostructures with high spin Hall conductivity, Nat. Mater. **23**, 768 (2024).

[52] T. Nan, C. X. Quintela, J. Irwin, G. Gurung, D. F. Shao, J. Gibbons, N. Campbell, K. Song, S.-Y. Choi, L. Guo *et al.*, Controlling spin current polarization through non-collinear antiferromagnetism, Nat. Commun. **11**, 4671 (2020).

[53] A. Bose, N. J. Schreiber, R. Jain, D.-F. Shao, H. P. Nair, J. Sun, X. S. Zhang, D. A. Muller, E. Y. Tsymbal, D. G. Schlom *et al.*, Tilted spin current generated by the collinear antiferromagnet ruthenium dioxide, Nat. Electron. **5**, 267 (2022).

[54] S. Shi, J. Li, C. Hsu, K. Lee, Y. Wang, L. Yang, J. Wang, Q. Wang, H. Wu, W. Zhang *et al.*, Observation of the out-of-plane polarized spin current from CVD grown WTe_2, Adv. Quantum Technol. **4**, 2100038 (2021).